

## ORIGINAL ARTICLE

## On the extent of the moat flow in axisymmetric sunspots

M. Verma<sup>\*1</sup> | P. Kummerow<sup>1,2</sup> | C. Denker<sup>1</sup><sup>1</sup>Leibniz-Institut für Astrophysik Potsdam (AIP), Potsdam, Germany<sup>2</sup>Universität Potsdam, Institut für Physik und Astronomie, Potsdam, Germany

## Correspondence

\*Email: mverma@aip.de

## Present Address

M. Verma, Leibniz-Institut für Astrophysik Potsdam (AIP), An der Sternwarte 16, 14482 Potsdam, Germany

## Abstract

Unipolar, axisymmetric sunspots are figuratively called “theoretician’s sunspots” because their simplicity supposedly makes them more suitable for theoretical descriptions or numerical models. On 2013 November 18, a very large specimen (active region NOAA 11899) crossed the central meridian of the Sun. The moat flow associated with this very large spot is quantitatively compared to that of a medium and a small sunspot to determine the extent of the moat flow in different environments. We employ continuum images and magnetograms of the Helioseismic and Magnetic Imager (HMI) as well as extreme ultraviolet (EUV) images at  $\lambda 160$  nm of the Atmospheric Imaging Assembly (AIA), both on board the Solar Dynamics Observatory (SDO), to measure horizontal proper motions with Local Correlation Tracking (LCT) and flux transport velocities with the Differential Affine Velocity Estimator (DAVE). We compute time-averaged flow maps ( $\pm 6$  hours around meridian passage) and radial averages of photometric, magnetic and flow properties. Flow fields of a small- and a medium-sized axisymmetric sunspot provide the context for interpreting the results. All sunspots show the outward moat flow and the advection of moving magnetic features (MMFs). However, the extent of the moat flow varies from spot to spot but a correlation of flow properties with size is tenuous, if at all present. The moat flow is asymmetric and predominantly in the east-west direction, whereby deviations are related to the tilt angle of the sunspot group as well as to the topology and activity level of the trailing plage.

## KEYWORDS:

sunspots – activity – photosphere – data analysis – image processing

## INTRODUCTION

Sunspots are surrounded by an annular horizontal flow field, the ‘moat flow’, which was first detected by [Sheeley \(1972\)](#). The moat flow was soon linked to sunspot decay ([Harvey & Harvey, 1973](#)), where MMFs ([Hagenaar & Shine, 2005](#)) play an important role in transporting magnetic flux across the spot’s boundary. Even residual pores, i.e., sunspots having lost their penumbrae, still exhibit MMFs and indications of moat flow ([Deng et al., 2007](#); [Verma et al., 2012](#); [Zuccarello et al., 2009](#)). However, the congruity between moat flow and sunspot

decay is challenged by its absence around many pores ([Cabrera Solana, Bellot Rubio, Beck, & del Toro Iniesta, 2006](#); [Vargas Domínguez et al., 2007](#)) and its presence in earlier stages of sunspot evolution ([Brickhouse & Labonte, 1988](#)). Thus, even four decades after discovery, fundamental questions remain open regarding the moat flow’s origin and its relation to the spot’s evolutionary stage, size, and penumbral dimensions.

Another outward radial flow starting at the sunspot’s penumbra is the Evershed flow ([Evershed, 1909](#)). The Evershed flow is correlated with the inclination angle and horizontal strength of the penumbral magnetic field (see [Deng, Shimizu, Choudhary, & Wang, 2011](#), for a sample of nine sunspots). A similar correlation holds for averaged quantities including the

total magnetic field strength with respect to the width of the penumbra. The relation between the Evershed flow and MMFs was studied by [Cabrera Solana et al. \(2006\)](#) who analyzed spectropolarimetric measurements of a sunspot in the Fe I  $\lambda 630.2$  nm and  $\lambda 1565$  nm lines. They followed the temporal evolution of radially outward moving Evershed clouds along the same penumbral filament. They concluded that the extension of the penumbral Evershed flow may appear as MMFs in the moat flow. [Rempel \(2011b\)](#) explained the relationship between moat and Evershed flow by suggesting two components of penumbral flows, one (deep) related to the moat flow and another (shallow) carrying the Evershed flow.

[Löhner-Böttcher & Schlichenmaier \(2013\)](#) used HMI Doppler maps to study moat and Evershed flow around 31 sunspots. From their analysis of three-hour averaged Doppler maps, they found that the moat flow velocity and its extent is independent of sunspot size. In contrast, they noticed an enhancement in the Evershed velocity with sunspot size. However, following the evolution of flows around long-lived sunspots for six to eight days, they observed an increase in the moat flow velocity along with the decay of sunspots. In contrast, the Evershed flow velocity decreased. They concluded that the moat flow is a non-magnetic flow deeper in the photosphere, whereas the Evershed flow is a magnetized flow extending into the sunspot canopy. They regarded MMFs to be advected by the moat flow but they consider these two phenomena to be different. Their view is in agreement with the work of [Nye, Bruning, & Labonte \(1988\)](#) who used linear numerical models of mass and energy flow suggesting that the driving force behind the moat flow is the stored thermal energy blocked by the sunspot. They also postulated that the moat flow's extent is proportional to the depth of sunspot penumbra but not to the size of sunspot.

[Weiss, Thomas, Brummell, & Tobias \(2004\)](#) suggested that magnetic flux tubes are dragged downward as a result of turbulent pumping by granular convection in the immediate surroundings of the sunspot (the “moat”), resulting in various types of MMFs. [Gafeira, Fonte, Pais, & Fernandes \(2014\)](#) presented another scenario, in which the velocity field interacts with an axially symmetric and height-invariant magnetic field, reproducing the large-scale features of the much more complex convection observed inside sunspots. Their results were in agreement with the Sun's subsurface dynamics ([Kitiashvili, Kosovichev, Wray, & Mansour, 2009](#)), where low-magnitude inflows of umbral and penumbral features can coexist with Evershed outflows as part of overturning convective motions.

Based on EUV  $\lambda 170$  nm and continuum images of the Transition Region and Coronal Explorer (TRACE, [Handy et al., 1999](#)), [Balthasar & Muglach \(2010\)](#) inferred the height dependence of the moat flow. In the upper atmosphere, flow speeds exceeded photospheric values in the inner moat while falling

**TABLE 1** Active region summary (area and radius).

NOAA	11809	12032	11899
Date	2013-08-06	2014-04-13	2013-11-18
Meridian passage	23:13 UT	18:06 UT	15:44 UT
$\mu = \cos \theta$	0.973	0.987	0.994
Area [Mm <sup>2</sup> ]			
$A_{\text{moat}}$	1102	1600	5188
$A_{\text{mag}}$	241	608	2231
$A_{\text{spot}}$	216	626	2266
$A_{\text{umbra}}$	41	128	586
Radius [Mm]			
$r_{\text{moat}}$	18.7	22.6	40.6
$r_{\text{mag}}$	8.8	13.9	26.7
$r_{\text{spot}}$	8.3	14.1	26.9
$r_{\text{umbra}}$	3.6	6.4	13.7

behind in the outer moat, which was attributed to a decoupling of the EUV bright-points from the photospheric plasma motions. However, [Sobotka & Roudier \(2007\)](#) observed that the moat areas are correlated in white-light and EUV images, but moat widths are independent of the spot radius (cf., [Brickhouse & Labonte, 1988](#)). In addition, an East-West asymmetry was observed, i.e., in white-light images the moat extended more in towards the East. However, this trend is opposite for the moat as seen in the EUV images.

## 1 | OBSERVATIONS AND DATA REDUCTION

On 2013 November 18, a large unipolar, axisymmetric sunspot crossed the central meridian of the Sun. Its exceptional size raises the question, if its horizontal flow field shows any peculiarities as compared to small- or intermediate-sized spots. We present preliminary results of an ongoing statistical study by focusing on three exemplary sunspots observed in 2013 and 2014 (see Table 1). The SDO data ([Pesnell, Thompson, & Chamberlin, 2012](#)) consist of HMI continuum images and magnetograms ([Scherrer et al., 2012](#); [Schou et al., 2012](#)) with a cadence of 45 s and AIA EUV  $\lambda 160$  nm images with 24-second sampling ([Lemen et al., 2012](#)), i.e., half of the fastest cadence of 12 s. Each image or magnetogram of the 12-hour time-series is compensated for differential rotation using the meridian passage of the spot as time reference. A region-of-interest (ROI) is extracted from the full-disk data, which is corrected for limb darkening (only continuum and EUV images) and geometric foreshortening. Thus, the intensity  $I$  is normalized to the local intensity of the quiet Sun, i.e.,  $I_{\text{con}}/I_0$  and  $I_{\text{EUV}}/I_0$ . The cross-correlation between single continuum images and their 12-hour average identifies residual drifts, associated with

active-region evolution, which are subsequently removed from all time-series. Resampling on a regular grid with a spacing of 0.4 Mm yields an ROI with dimensions of 160 Mm  $\times$  160 Mm. The data processing essentially follows the procedures elaborated in Kummerow (2015), Verma & Denker (2011), and Beauregard, Verma, & Denker (2012).

Continuum and EUV images are subjected to the LCT algorithm outlined in Verma & Denker (2011), which is a variant of the technique put forward by November & Simon (1988). A subsonic filter with a cut-off at the photospheric sound speed suppresses intensity variations caused by solar oscillations. Sampling window and high-pass filter are identical and have a size of 6.4 Mm  $\times$  6.4 Mm. They are implemented as two-dimensional Gaussians with a full-width-at-half-maximum of 2 Mm. The cadence for correlating image pairs is  $\Delta t = 90$  s and 96 s for continuum and EUV images, respectively. Individual flow maps are averaged over  $\Delta T = 12$  hours to derive the persistent flows in and around sunspots.

Flux transport velocities are derived from magnetograms using DAVE (Schuck, 2005, 2006) with a 11 $\times$ 11-pixel (4.4 Mm  $\times$  4.4 Mm) sampling window. We coarsely assume that the magnetic field lines are perpendicular to the solar surface, thus, dividing the field strength  $B_{\text{LOS}}$  along the line-of-sight (LOS) by the cosine of the heliocentric angle  $\mu$  yields  $B = B_{\text{LOS}}/\mu$ . Convolving the magnetograms with the appropriate Scharr (2007) operators results in the spatial derivatives of the magnetic field in the  $x$ - and  $y$ -directions, whereas the temporal derivative is based on a five-point stencil with a 15-minute time interval. Taking into account the 30-minute offsets at the beginning and end of the time-series because of the five-point stencil, 880 individual flow maps enter the computation of the time-averaged flow maps.

## 2 | RESULTS

The three sunspots are chosen as representative examples for small, medium, and large sunspots. Morphological image processing and thresholding provide areas  $A$  enclosed by the spot's photometric, magnetic, and moat boundaries. Equivalent radii  $r$  refer to circles that conform to the respective perimeters. To measure the sunspot's area, the average continuum image is smoothed using a Perona-Malik filter (Perona & Malik, 1990), and fixed intensity thresholds of  $I_{\text{con}}/I_0 = 0.6$  and  $I_{\text{con}}/I_0 = 0.92$  are applied to determine the extent of umbra and penumbra, respectively. The area and radius are then estimated using the blob-analyzer code by Fanning (2003) as described in Verma & Denker (2014). Magnetic area and radius are computed by thresholding the magnitude of the magnetograms at  $B = 100$  G. The areal extent of the moat is computed using DAVE velocity maps, where morphological

smoothing is applied to the radial component of the velocity, along with a threshold of 100 m s $^{-1}$  for the radial velocity. We compare the moat's extent based on radial velocity maps for continuum and EUV images, but only the results from magnetograms led to a robust estimate for the moat's area. Area and radius for the three sunspots are listed in Table 1. In the remainder of this study, the physical parameters characterizing the flow fields refer to the feature definitions above.

Maps depicting time-averaged horizontal proper motions and flux transport velocities are compiled in Fig. 1 for active regions NOAA 11809, 12032, and 11899, which exemplarily displays a small, a medium, and a large sunspot, respectively. The background images are continuum images, EUV images, and magnetograms at meridian passage. Flow vectors exist for each of the 400  $\times$  400 pixels in the FOV but for display purposes the flow vectors are resampled onto an equidistant grid of 60  $\times$  60 points. However, quantitative flow speeds always refer to averages over all pixels belonging to a certain feature.

Spatial resolution and contrast of continuum images are sufficient to measure persistent flows in the granulation. Thus, the continuum flow maps contain additionally signatures of meso- and supergranular flows (November & Simon, 1988). Furthermore, prominent circles with close to zero flow speeds (Deng et al., 2007; Denker, 1998; Molowny-Horas, 1994) are visible in the middle of the penumbra (divergence) and at the termination of the moat flow (convergence). Even though we select unipolar, axisymmetric sunspots, the flow fields exhibit significant asymmetries (see e.g., Sobotka & Roudier, 2007). For all three sunspots the moat flows are lower on the south-west side.

The velocities patterns seen in the flow maps based on magnetograms are virtually identical to those based on continuum images, except the pronounced meso- and supergranular pattern is absent, and the flow field around the sunspot is more cohesive. Therefore, the moat flow is much easier discernible in these maps depicting flux transport velocities, and the aforementioned asymmetries are also present. In EUV images, the contrast of bright-points belonging to the chromospheric network and decaying plage is even higher – exceeding the granular contrast by far. The flow maps based on EUV images show that the horizontal proper motions are suppressed in the plage regions, i.e., at the location of dispersed small-scale magnetic flux elements. However, taking into account the entire quiet Sun, the flow speeds are highest for the EUV flow maps. Furthermore, the moat flow is more symmetric in EUV flow maps as compared to flow maps based on continuum images and magnetograms.

The photometric and magnetic radii are virtually identical. These radii are about 8.5, 14, and 27 Mm for the three sunspots, whereas the areas are about 230, 620, and 2250 Mm $^2$ . The respective moat areas are about 1100, 1600, and 5200 Mm $^2$ . These values show that the moat area is about two times larger



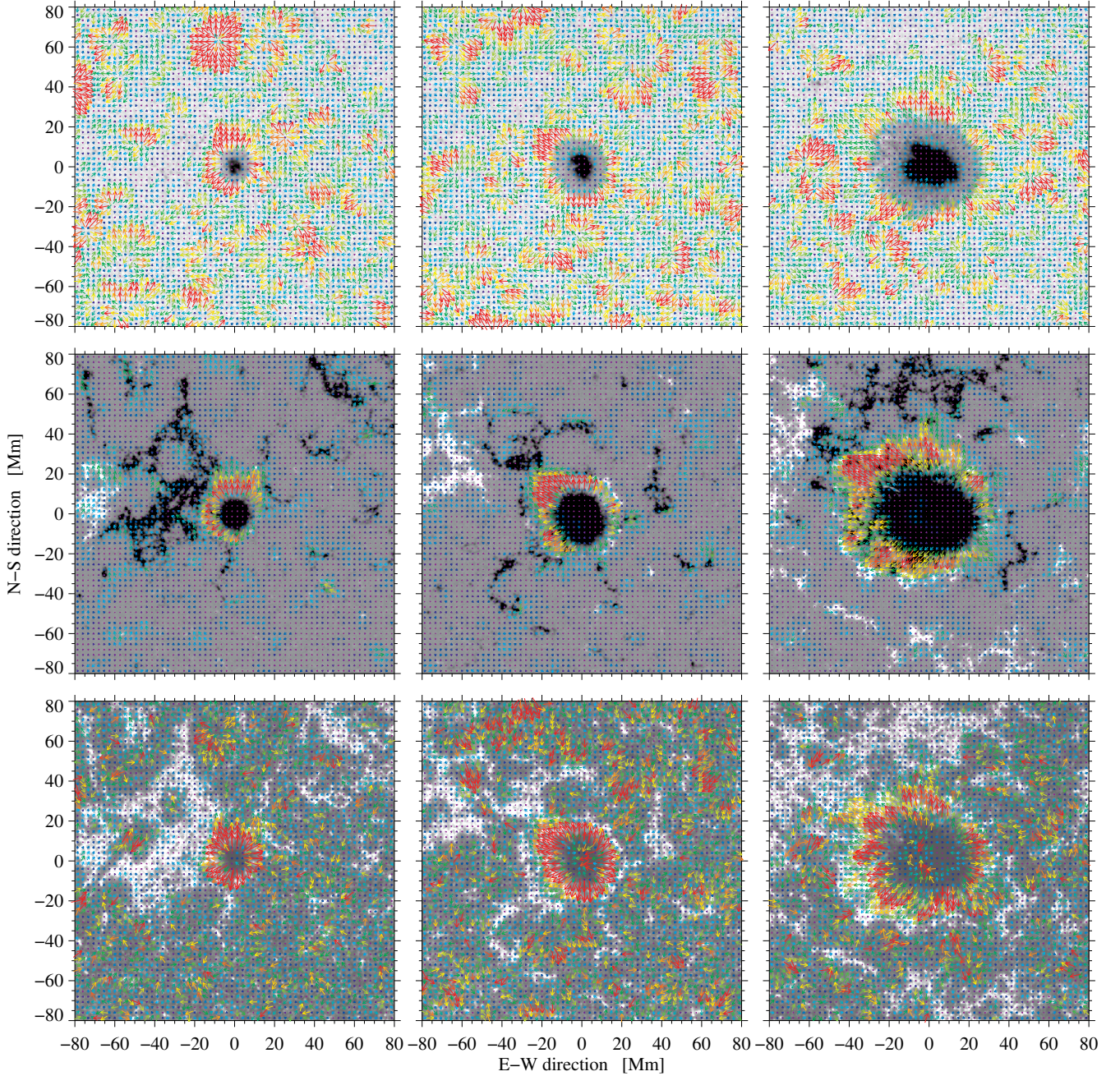


**FIGURE 1** Continuum intensity  $I_{\text{con}}/I_0$ , magnetic flux density  $B = B_{\text{LOS}}/\mu$ , and EUV intensity  $I_{\text{EUV}}/I_0$  (top to bottom) for three axisymmetric sunspots in active regions NOAA 11809, 12032, and 11899 (left to right), respectively. The superimposed, rainbow-colored vectors represent magnitude and direction of the horizontal proper motions. Violet and red correspond in the top panels to flow speeds of lower than  $0.05$  and larger than  $0.25 \text{ km s}^{-1}$ , respectively. Scaling this range by factors of  $1.6$  and  $2.0$ , respectively, accommodates the higher flow speeds derived from magnetograms and EUV images.

than the spot area for the medium and large sunspot, whereas the moat area is almost five times larger for the small sunspot. Expressing these findings in terms of the radius, the ratios of moat to spot radius  $r_{\text{moat}}/r_{\text{spot}}$  are  $2.3$ ,  $1.6$ , and  $1.5$  for the small, medium, and large spot, respectively.

To quantify the flow properties, we compile the mean flow speeds for moat, penumbra, umbra, and quiet Sun in Table 2. The mean flux transport velocities are higher in the moat for all three spots, followed closely by the horizontal proper motions derived from EUV images. The flow speeds for penumbra and

**TABLE 2** Active region summary (horizontal proper motions and flux transport velocities).

Features	Continuum $\bar{v} \pm \sigma_v$ [m s <sup>-1</sup> ]	Magnetogram $\bar{v} \pm \sigma_v$ [m s <sup>-1</sup> ]	EUV $\bar{v} \pm \sigma_v$ [m s <sup>-1</sup> ]
<b>11809</b>			
Moat	165 ± 117	277 ± 94	221 ± 152
Penumbra	66 ± 56	45 ± 27	166 ± 168
Umbra	24 ± 20	34 ± 7	130 ± 90
Quiet Sun	142 ± 102	82 ± 47	162 ± 129
<b>12032</b>			
Moat	219 ± 123	312 ± 109	267 ± 155
Penumbra	95 ± 71	97 ± 79	228 ± 188
Umbra	46 ± 35	41 ± 23	279 ± 204
Quiet Sun	149 ± 104	75 ± 44	175 ± 132
<b>11899</b>			
Moat	131 ± 101	221 ± 132	179 ± 122
Penumbra	90 ± 75	165 ± 109	182 ± 147
Umbra	50 ± 41	54 ± 27	167 ± 132
Quiet Sun	132 ± 91	77 ± 46	150 ± 126

umbra are virtually identical for flow maps based on continuum images and magnetograms, whereas they are higher for maps based on EUV images. The quiet-Sun flow speeds for continuum and EUV maps are of the same order while the flux transport velocities are smaller. A likely explanation is that DAVE does not track very faint, small-scale magnetic elements in the quiet Sun. Interestingly, the flow speed in the moat is highest for the medium-sized sunspot and lowest for the large sunspot in all three types of flow maps. Although, this discrepancy is most evident in the flow speeds and flux transport velocities derived from continuum images and magnetograms, respectively.

Radial averages of sunspot properties facilitate an easier comparison of sunspots with different sizes. In this sense, Fig. 2 complements the two-dimensional maps of Fig. 1, and we introduce additional parameters describing the flow field. The horizontal velocity vector  $\vec{v} = (v_x, v_y)$  is decomposed yielding the radial component of the flow velocity  $u = v_x \cos \varphi + v_y \sin \varphi$ , where  $\varphi$  is the azimuth about the spot's center measured counterclockwise from west (positive  $x$ -axis). The divergence  $\nabla \cdot \vec{v} = \partial v_x / \partial x + \partial v_y / \partial y$  is computed using finite differences. Table 3 lists the characteristic values for the averaged radial profiles of various physical parameters shown in Fig. 2 along with the corresponding radial distance from the center of the spots.

Inspecting radial profiles for axisymmetric sunspots motivates different definitions of thresholds for features using inflection points and extreme values. The continuum radius  $I_{\text{con}}/I_0 = 1$  and magnetic radius  $B = 50$  G are virtually identical with about 10, 16, and 32 Mm for the small, medium, and large sunspot, respectively. The radii derived from azimuthal

**TABLE 3** Active region summary (radial distance to maximum values).

Parameters	Continuum	Magnetogram	EUV
<b>11809</b>			
$I_{\text{max}}/I_0, B_{\text{max}}$ [G]	1.0 10.0	50 10.0	1.7 11.2
$v$ [km s <sup>-1</sup> ]	0.42 11.2	0.36 12.4	0.63 9.2
$u_{\text{rad}}$ [km s <sup>-1</sup> ]	0.42 11.2	0.34 12.4	0.62 9.2
$\nabla \cdot \vec{v}$ [ $\times 10^{-2}$ s <sup>-1</sup> ]	0.056 8.0	0.046 9.6	0.10 7.6
<b>12032</b>			
$I_{\text{max}}/I_0, B_{\text{max}}$ [G]	1.0 16.4	50 16.0	1.7 18.4
$v_{\text{rad}}$ [km s <sup>-1</sup> ]	0.36 16.8	0.31 17.2	0.59 14.4
$u_{\text{rad}}$ [km s <sup>-1</sup> ]	0.36 16.4	0.30 17.2	0.58 14.4
$\nabla \cdot \vec{v}$ [ $\times 10^{-2}$ s <sup>-1</sup> ]	0.038 11.2	0.027 13.6	0.067 11.2
<b>11899</b>			
$I_{\text{max}}/I_0, B_{\text{max}}$ [G]	1.0 31.6	50 28.8	1.5 30.8
$v_{\text{rad}}$ [km s <sup>-1</sup> ]	0.30 28.8	0.31 28.0	0.36 25.6
$u_{\text{rad}}$ [km s <sup>-1</sup> ]	0.29 28.8	0.30 28.4	0.34 25.6
$\nabla \cdot \vec{v}$ [ $\times 10^{-2}$ s <sup>-1</sup> ]	0.019 20.8	0.016 23.6	0.029 17.6

Note:  $v$  is the flow speed,  $u_{\text{rad}}$  is the radial flow speed, and  $\nabla \cdot \vec{v}$  is the divergence. The values below the physical parameters refer to the radial distance in megameters.

averages are somewhat larger than those based on thresholds for two-dimensional maps of intensity and magnetic field. The normalized EUV intensity has two peaks. One at the location matching the continuum and magnetic radii, and a secondary peak further out. The first peak is the prominent one for the medium and large sunspot, but not for the small sunspot, where the secondary peak is stronger. The secondary peaks are mainly caused by EUV bright-points. The flow speed based on continuum images and magnetograms peaks at the location of the continuum and magnetic boundaries for all sunspots. In the EUV, we find a peak just before the continuum and magnetic boundaries.

Azimuthal averages of the radial flow speed have a similar trend for horizontal proper motions based on the continuum images for all sunspots. In the spot's center the radial flow speed is zero, but starts to decrease (negative speed indicates inflows) reaching a minimum at around the radial distance that corresponds to  $I_{\text{con}}/I_0 \approx 0.6$ . The radial flow speed returns to



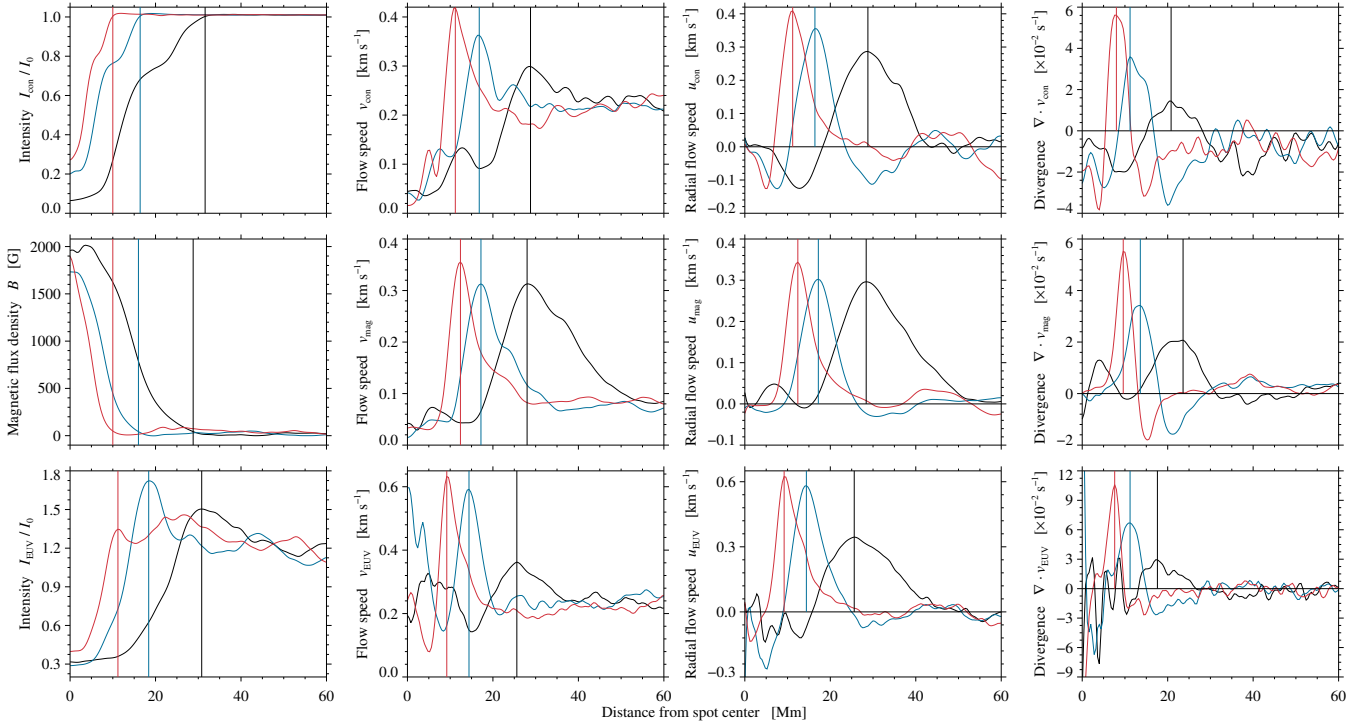


**FIGURE 2** Radial averages of intensity  $I$ , magnetic flux density  $B$ , horizontal flow speed  $v$ , radial component of the flow speed  $u$ , and divergence  $\nabla \cdot v$  (left to right). The profiles are based on continuum images, magnetograms, and EUV images (top to bottom). Red, blue, and black lines refer to active regions NOAA 11809, 12032, and 11899, respectively. The vertical lines mark characteristic parameters of the displayed radial profiles and the corresponding radial distances from the center of the spots, which are summarized in Table 3.

zero inside the penumbra at  $I_{\text{con}}/I_0 \approx 0.7$ . The negative radial flow speed is caused by inward migrating penumbral grains with high contrasts and may not reflect a real plasma motion. The maximum of the radial flow speed is reached  $I_{\text{con}}/I_0 \approx 1$ . Moreover, the radial flow speeds based on magnetograms and EUV images follow a similar trend deviating only inside the spots, where the radial flow speeds are much noisier.

In the continuum, the divergence is negative inside the three sunspots, similar to the radial flow speed. The divergence switches to positive value inside the sunspots before attaining a maximum. The location, where the divergence reaches its maximum, is inside the spot's penumbra. Once the maximum is reached the divergence slowly approaches zero. Outside sunspots the divergence fluctuates between small positive and negative values.

To quantitatively assess asymmetries in the moat flow, we plot the radial velocity separately for East and West sides of the three sunspots and the three data types in Fig. 3. Asymmetric flows appear for the east component as broader profiles with maxima shifted further out. However, the width of the profiles is the distinguishing characteristic, whereas the displacement of the maxima is less pronounced. The largest displacement of

about 8 Mm is observed for the largest sunspot. In most cases, the values of maxima are virtually identical for both sides, except for the small and medium sunspots, where the east side exhibits higher values for radial continuum and flux transport velocities. This East-West asymmetry in the moat flow was also observed by Kummerow (2015) in the averaged flow field maps of 26 sunspots, corroborating the findings of Sobotka & Roudier (2007).

For all three sunspots, we plot the background-subtracted variation of the magnetic flux density  $\langle |B - \langle B \rangle| \rangle$  and the EUV intensity  $\langle |I - \langle I \rangle| \rangle$  (Fig. 4). In all three cases, the sunspots occupy the center of a supergranular cell. Spoke-like structures join the sunspots to the surrounding supergranular network, as is evident in the variation of magnetic flux density and EUV intensity. This kind of radial structure was first reported by Verma et al. (2012) around a decaying sunspot. The length of these spokes varies for all three sunspots. They are longest for the large sunspot, where the length of the spokes varies between 15–20 Mm. An east-west asymmetry is present in the medium and large sunspot, with longer spokes extending towards the east. The variation maps are a versatile tool to visualize ongoing changes in active regions. They also clearly

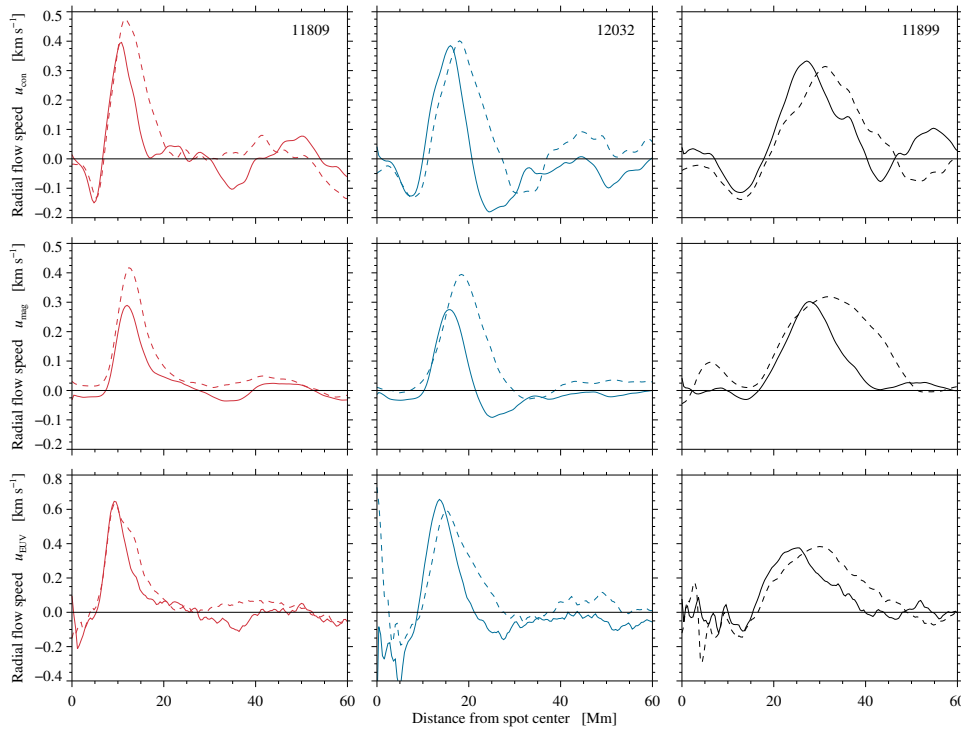


**FIGURE 3** The east (*dashed*) and west (*solid*) components of radial velocities based on continuum images, magnetograms, and EUV images (*top to bottom*). Red, blue, and black lines refer to active regions NOAA 11809, 12032, and 11899, respectively.

demonstrate the connectivity of horizontal proper motions and flux transport velocities within the entire active region.

### 3 | DISCUSSION AND CONCLUSIONS

Three axisymmetric sunspots with different radii were selected to scrutinize horizontal proper motions based on continuum and EUV images (LCT) and flux transport velocities based on magnetograms (DAVE). Our study complements the work by [Löhner-Böttcher & Schlichenmaier \(2013\)](#), which was based on HMI Doppler maps. In proximity to the solar limb, horizontal flows in and around sunspots can be determined by decomposing the Doppler velocity. In contrast, our measurements yield horizontal flows in and around sunspots in proximity to the disk center. [Löhner-Böttcher & Schlichenmaier \(2013\)](#) found that the moat flow size and velocities are independent of the sunspot size, similar to previous work by [Sobotka & Roudier \(2007\)](#). In addition, the former authors concluded that MMFs are related to the inclined magnetic field lines (relative to horizontal), and although they are advected by the moat flow, they are distinguishable from it. In the present work, the moat radius of the small sunspot is 2.25 times the photometric radius, whereas for the medium and large sunspot it is 1.6 and 1.5 times the photometric radius, respectively. Hence, we also do not find any clear relation between the photometric and the

moat radius. Even the much larger sample of 26 sunspots scrutinized by [Kummerow \(2015\)](#) shows only a tenuous correlation between sunspot and moat radius, if at all.

Large, isolated, axisymmetric sunspots are more likely to emerge at low latitudes during the declining phase of the solar cycle ([Koutchmy & Le Piouffle, 2009](#)). The large sunspot of this study was chosen as an example from the declining phase of solar cycle No. 24. A medium and a small sunspot were used for comparison. The horizontal flow properties in the continuum were similar for all three spots, with an outflow encircling the spots and inflows in the inner penumbra. The basic properties of the moat flow remained the same irrespective of the spot's size. An east-west asymmetry of moat flow was observed for all spots, which however was more prominent in the flow maps based on continuum images and magnetograms. This result is in agreement with the work of [Sobotka & Roudier \(2007\)](#). However, in a case study, [Balthasar et al. \(2009\)](#) did not find any asymmetry in the moat flow, when a sunspot was observed in both white-light and EUV images.

The asymmetric moat flow is not strictly oriented in the east-west direction. Thus, the tilt angle of the active region and the distribution of the neighboring plage may significantly impact the orientation. The overall topology of leading axisymmetric sunspots and trailing plage regions may also affect the height-dependent moat flow observed in continuum and EUV flow maps. Moreover, the maps of the EUV intensity and magnetic field variation show that the moat region is most “active” for the large spot, whereas the plage regions of the small and

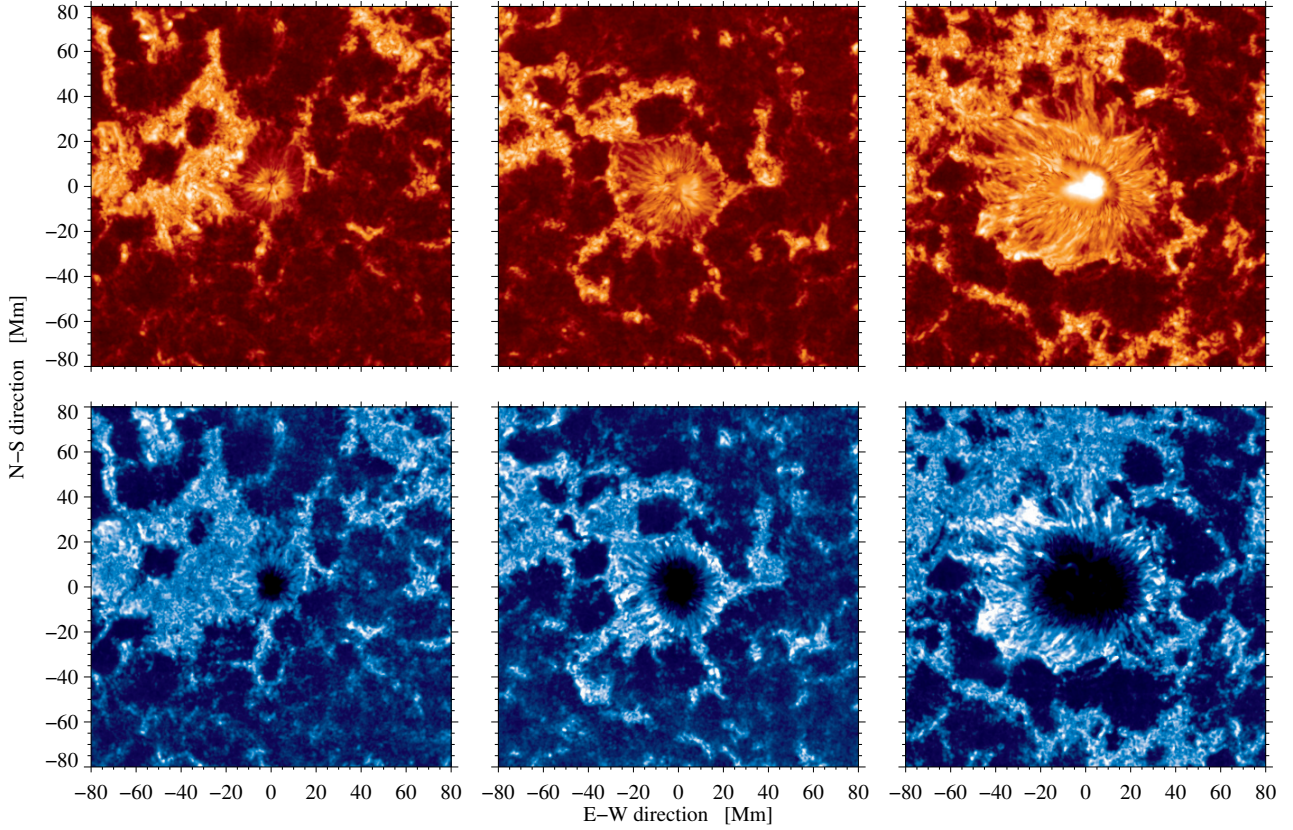


**FIGURE 4** Background-subtracted variations of the magnetic flux density (*top*)  $\langle |B - \langle B \rangle| \rangle$  and the EUV intensity (*bottom*)  $\langle |I - \langle I \rangle| \rangle$  in active regions NOAA 11809, 12032, and 11899 (*left to right*), where  $\langle \dots \rangle$  indicates an ensemble average (logarithmic display).

medium spots show enhanced activity. Is this an indication that these spots are stable and that the evolution of the active region is governed by the trailing plage? The strongest EUV variations are seen for the large sunspot on the eastern side. Here, the spot is most closely connected to the trailing plage. Addressing these issues will be deferred to a forthcoming more comprehensive statistical study encompassing all available SDO data.

The EUV continuum ( $\lambda 160$  nm) forms just below the temperature minimum about 450–500 km above the photosphere (Vernazza, Avrett, & Loeser, 1981). Hence, computing proper motions based on EUV images gives access to higher atmospheric layers. This approach has already been followed by Sobotka & Roudier (2007) and Balthasar et al. (2009), when they used TRACE white-light and EUV images. In the azimuthally averaged intensity around the three sunspots in the current study, a peak appears in EUV similar to what was observed by Balthasar et al. (2009). This indicates the presence of long-lived, small-scale bright-points around sunspots,

which appear higher in the atmosphere. The moat flow itself was well traceable in the EUV images. Flux transport velocities were computed with DAVE, which match the horizontal proper motions derived from continuum images. However, the typical inward motion in the inner penumbra is absent in the flux transport velocities. A likely explanation is the inward motion of penumbral grains visible in time-series of continuum images. These can be interpreted as the footpoints of flux tubes, which become more vertical so that the bright footpoints migrate inwards (Schlichenmaier, Jahn, & Schmidt, 1998a, 1998b). Such a phase velocity resulting from systematic contrast changes will not be picked up by DAVE.

Švanda, Sobotka, & Bárta (2014) applied time-distance helioseismic inversions to study the properties of sub-surface moat flows in 104 H-class sunspots and over 200 000 supergranule cells. Even though, they found similarities in both flows, and the moat flows replace the supergranular flows around H-class sunspot, there are two major differences. First, the moat flow is asymmetric due to the sunspot motion across



the solar disk and is disturbed by the surrounding plasma resulting in a larger extension on the eastern side than on the western side. In contrast, the outflow region in supergranules is symmetric. Second, studying the vertical flows, they noticed that the moat regions exhibit exclusively downflows, whereas supergranules have upflows in the center which turn into downflows at 60% cell radius. This is related to mass sinking down around the H-sunspot in a shallow sub-surface layer, which is at least twice the mass submerging on average in supergranular cells.

The horizontal flow properties around pores were summarized by Verma & Denker (2014). The radial average of the horizontal velocities revealed that pores, i.e., spots which never developed a penumbra, have a moat-like outflow structure encircling them. Moat flows are also seen around decaying sunspots (e.g., Balthasar et al., 2013; Verma et al., 2012) – even when the sunspot shrunk to become a residual pore, i.e., losing its penumbra. This raises the question, is a penumbra needed for setting up moat flows or is the moat flow a part of an even larger flux system? In a recent study, Strecker (2015) raised the question if the moat flow is embedded in a cell of the supergranular network. She employed the method described by Löhner-Böttcher & Schlichenmaier (2013) to compute horizontal proper motions for eight sunspots from limb-to-limb. By following the evolution of horizontal velocity she concluded that there is a constant interaction between moat flows and the surrounding supergranular cells at all stages of sunspot evolution. Maps of the EUV intensity and the magnetic field variation exhibit EUV bright-points and magnetic features, which migrate from all three sunspots towards the surrounding network. These easily perceived, radial paths are followed by the MMFs and overlap with the encircling moat flow. Verma et al. (2012) already identified these radial spokes around a decaying sunspot. However, in the present study, none of the sunspots were decaying but they all were in a rather mature state. This clearly demonstrates that sunspots are part of a larger magnetic flux system, which encompasses an entire supergranular cell.

In recent work, Rempel (2011a) and Rempel (2015) investigated the relationship between moat and Evershed flow. Three magnetic components are involved in the flow patterns associated with sunspots: (1) the horizontal field leading to magnetized horizontal flows, (2) the vertical field that does not possess a horizontal flow component, and (3) the deep non-magnetized flows that predominantly contribute to the moat flow. In conclusion, the Evershed flow is a magnetized flow because of the inclined magnetic fields and the overturning convection, whereas the moat flow results from a perturbation of the up- and downflow balance around the spot. In the present study, we confirm that certain flow properties are common for sunspots irrespective of their size, e.g., the outward

moat flow and the advected MMFs. The properties of moat flow vary from spot to spot, but the overall trend remains the same. The MMFs moved to the surrounding network in all the three sunspots and are partly carried by the encircling moat.

The uniformity of HMI and AIA data facilitates a quantitative comparison of sunspots, among others, of different size and evolutionary stage – even statistical studies covering rise and fall of solar cycle No. 24 are now possible. We have presented numerical methods and analysis tool, which allowed us to compare the flow properties of “theoretician’s sunspots” from the smallest spots to one of the largest specimen. The radial velocity profiles and the background-subtracted solar activity maps for magnetograms and EUV intensity have proven very versatile in establishing the connection between the sunspots and the surrounding supergranular cells, which deserve a holistic treatment in modeling.

## ACKNOWLEDGMENTS

SDO HMI and AIA data are provided by the Joint Science Operations Center – Science Data Processing. MV and CD acknowledge support by grant DE 787/5-1 of the German Science Foundation (DFG).

## REFERENCES

- Balthasar, H., Beck, C., Gömöry, P., Muglach, K., Puschmann, K. G., Shimizu, T., & Verma, M. 2013, *Centr. Eur. Astrophys. Bull.*, 37, 435.
- Balthasar, H., Bello González, N., Collados, M., Denker, C., Hofmann, A., Kneer, F., & Puschmann, K. G. 2009, A Full-Stokes Polarimeter for the GREGOR Fabry-Pérot Interferometer. K. G. Strassmeier, A. G. Kosovichev, & J. E. Beckmann (Eds.), *Cosmic Magnetic Fields: From Planets, to Stars and Galaxies* Vol. 259, p. 665-666.
- Balthasar, H., & Muglach, K. 2010, *A&A*, 511, A67.
- Beauregard, L., Verma, M., & Denker, C. 2012, *AN*, 333.
- Brickhouse, N. S., & Labonte, B. J. 1988, *SoPh*, 115, 43-60.
- Cabrera Solana, D., Bellot Rubio, L. R., Beck, C., & del Toro Iniesta, J. C. 2006, *ApJL*, 649, L41-L44.
- Deng, N., Choudhary, D. P., Tritschler, A., Denker, C., Liu, C., & Wang, H. 2007, *ApJ*, 671, 1013-1021.
- Deng, N., Shimizu, T., Choudhary, D. P., & Wang, H. 2011, What Determines the Penumbra Size and Evershed Flow Speed? D. Prasad Choudhary & K. G. Strassmeier (Eds.), *Physics of Sun and Star Spots* Vol. 273, p. 216-220.
- Denker, C. 1998, *SoPh*, 180, 81-108.
- Evershed, J. 1909, *Mon. Not. R. Astron. Soc.*, 69, 454-457.
- Fanning, D. W. 2003, *IDL Programming Techniques* (Second ed.), Fort Collins, Co.: Fanning Software Consulting.
- Gafeira, R., Fonte, C. C., Pais, M. A., & Fernandes, J. 2014, *SoPh*, 289, 1531-1542.
- Hagenaar, H. J., & Shine, R. A. 2005, *ApJ*, 635, 659-669.
- Handy, B. N., Acton, L. W., Kankelborg, C. C. et al. 1999, *SoPh*, 187, 229-260.

- Harvey, K., & Harvey, J. 1973, *SoPh*, 28, 61-71.
- Kitiashvili, I. N., Kosovichev, A. G., Wray, A. A., & Mansour, N. N. 2009, *ApJL*, 700, L178-L181.
- Koutchmy, S., & Le Piuille, V. 2009, Isolated Quasi-Axisymmetric sunspots. K. G. Strassmeier, A. G. Kosovichev, & J. E. Beckman (Eds.), *Cosmic Magnetic Fields: From Planets, to Stars and Galaxies* Vol. 259, p. 227-228.
- Kummerow, P. 2015. Vermessung der Horizontalen Strömungen in Sonnenflecken (Unpublished master's thesis). Potsdam.
- Lemen, J. R., Title, A. M., Akin, D. J. et al. 2012, *SoPh*, 275, 17-40.
- Löhner-Böttcher, J., & Schlichenmaier, R. 2013, *A&A*, 551, A105.
- Molowny-Horas, R. 1994, *SoPh*, 154, 29-39.
- November, L. J., & Simon, G. W. 1988, *ApJ*, 333, 427-442.
- Nye, A., Bruning, D., & Labonte, B. J. 1988, *SoPh*, 115, 251-268.
- Perona, P., & Malik, J. 1990, *IEEE Trans. Pattern Anal. Mach. Intell.*, 12, 629-639.
- Pesnell, W. D., Thompson, B. J., & Chamberlin, P. C. 2012, *SoPh*, 275, 3-15.
- Rempel, M. 2011a, *ApJ*, 729, 5-27.
- Rempel, M. 2011b, *ApJ*, 740, 15.
- Rempel, M. 2015, *ApJ*, 814, 125.
- Scharr, H. 2007, Optimal Filters for Extended Optical Flow. B. Jähne, R. Mester, B. Barth, et al. (Eds.), *Complex Motion* Vol. 3417, p. 14-29. Berlin: Springer.
- Scherrer, P. H., Schou, J., Bush, R. I. et al. 2012, *SoPh*, 275, 207-227.
- Schlichenmaier, R., Jahn, K., & Schmidt, H. U. 1998a, *ApJL*, 493, 121-124.
- Schlichenmaier, R., Jahn, K., & Schmidt, H. U. 1998b, *A&A*, 337, 897-910.
- Schou, J., Scherrer, P. H., Bush, R. I. et al. 2012, *SoPh*, 275, 229-259.
- Schuck, P. W. 2005, *ApJL*, 632, L53-L56.
- Schuck, P. W. 2006, *ApJ*, 646, 1358-1391.
- Sheeley, N. R., Jr. 1972, *SoPh*, 25, 98-103.
- Sobotka, M., & Roudier, T. 2007, *A&A*, 472, 277-282.
- Strecker, H. 2015. The Evolution of the Moat Flow around Sunspots: Is the Network Cell Hosting the Sunspot's Moat Cell? (Unpublished master's thesis). Universität Freiburg.
- Švanda, M., Sobotka, M., & Bárta, T. 2014, *ApJ*, 790, 135.
- Vargas Domínguez, S., Bonet, J. A., Martínez Pillet, V., Katsukawa, Y., Kitakoshi, Y., & Rouppe van der Voort, L. 2007, *ApJL*, 660, 165-168.
- Verma, M., Balthasar, H., Deng, N., Liu, C., Shimizu, T., Wang, H., & Denker, C. 2012, *A&A*, 538, A109.
- Verma, M., & Denker, C. 2011, *A&A*, 529, A153.
- Verma, M., & Denker, C. 2014, *A&A*, 563, A112.
- Vernazza, J. E., Avrett, E. H., & Loeser, R. 1981, *ApJSS*, 45, 635-725.
- Weiss, N. O., Thomas, J. H., Brummell, N. H., & Tobias, S. M. 2004, *ApJ*, 600, 1073-1090.
- Zuccarello, F., Romano, P., Guglielmino, S. L. et al. 2009, *A&A*, 500, L5-L8.

**How cite this article:** M. Verma, P. Kummerow, and C. Denker (2018), On the extent of the moat flow in axisymmetric sunspots, *ASNA*, 2018;00:1–8.

**How cite this article:** M. Verma, P. Kummerow, and C. Denker (2018), On the extent of the moat flow in axisymmetric sunspots, *ASNA*, 2018;00:1–8.